Supporting Information

Full complex-amplitude modulation of second harmonic generation with nonlinear metasurfaces

Zelin Hao, Wenwei Liu, Zhancheng Li, Zhi Li, Guangzhou Geng, Yanchun Wang, Hua Cheng, Hammad Ahmed, Xianzhong Chen, Junjie Li, Jianguo Tian*, and Shuqi Chen**

Dr. Z. Hao, Dr. W. Liu, Dr. Z. Li, Dr. Z. Li, Dr. G. Geng, Dr. Y. Wang, Prof. H. Cheng, Prof. J. Tian, Prof. S. Chen
The Key Laboratory of Weak Light Nonlinear Photonics, Ministry of Education, Renewable Energy Conversion and Storage Center, School of Physics and TEDA Institute of Applied Physics, Nankai University, Tianjin 300071, China
E-mail: hcheng@nankai.edu.cn; jjtian@nankai.edu.cn; schen@nankai.edu.cn
Prof. J. Li
Beijing National Laboratory for Condensed Matter Physics, Institute of Physics, Chinese Academy of Sciences, Beijing 100190, China
Dr. H. Ahmed, Prof. X. Chen
Institute of Photonics and Quantum Sciences, School of Engineering and Physical Sciences, Heriot-Watt University, Edinburgh, EH14 4AS, UK
Prof. S. Chen
The Collaborative Innovation Center of Extreme Optics, Shanxi University, Taiyuan, Shanxi 030006, China
Prof. S. Chen
Collaborative Innovation Center of Light Manipulations and Applications, Shandong Normal University, Jinan 250358, China

This file includes 6 pages and 5 figures

Section 1: The emitted second harmonic waves from a uniform array

Section 2. Wavelength-dependent SHG intensities of the designed C_3-symmetric nanoparticle

Section 3: The variations of the amplitude and phase of the generated SH waves with the structural rotation angle

Section 4: The calculated multichannel vortex beams generated by phase-only nonlinear metasurface

Section 5: Spin-selective generation of four SH optical vortices with independent topological charges

Section 6. The design of the spin-controlled multifunctional nonlinear metasurface

Section 1. The emitted second harmonic waves from a uniform array

The radiation of the second harmonic (SH) waves from a uniform array composed of C_3-symmetric nanoparticles were simulated based on the nonlinear surface currents. In the designed array, the C_3-symmetric nanoparticles are located at the centers of the hexagonal unit cells and the period between the nanoparticles is 600 nm. The simulated results in Figure S1 show that the SH waves, whose polarization state is opposite to that of the fundamental wave (FW), can radiate to the far field. Meanwhile, the co-polarized SH waves cannot radiate to the far field.

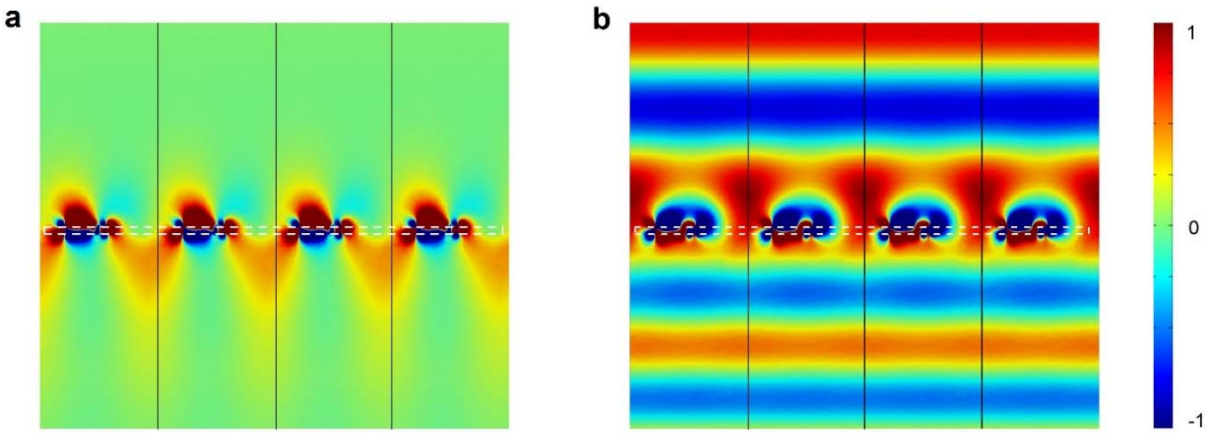

Figure S1. A time snapshot of the simulated electric fields for a) co-polarized SH waves. and b) cross-polarized SH waves under RCP illumination. The dotted box represents the position of the designed array.

Section 2. Wavelength-dependent SHG intensities of the designed C_3-symmetric nanoparticle

The calculated SHG intensities of the designed C_3-symmetric nanoparticle as a function of the fundamental wavelength are shown in Figure S2. The intensities of SHG waves with opposite optical spin to that of the fundamental waves are much stronger, as required by the selection rules for the harmonic generations.

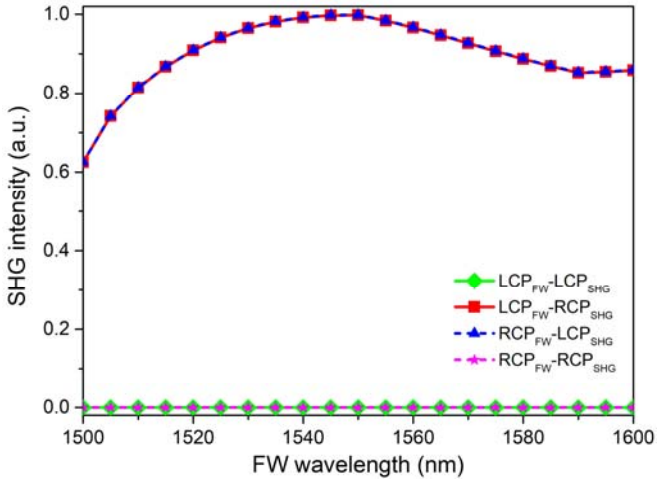

Figure S2. The calculated wavelength-dependent SHG intensities of the designed C_3-symmetric nanoparticle under the pumping of the LCP and RCP FWs.

Section 3. The variations of the amplitude and phase of the generated SH waves with the structural rotation angle

Figure S3 further proves that the rotation angle of the designed C_3-symmetric nanoparticle has negligible influence on the amplitude of the generated SH waves, while the phase of the generated SH waves linearly varies with the rotation angle. Moreover, the variation of the phase of the generated SH waves with the changing of the rotation angle of the designed C_3-symmetric nanoparticle satisfies a threefold relationship, that is the nonlinear geometry phase of the *n*th harmonic generation with opposite circular polarization to that of the fundamental wave is $(n+1)\sigma\theta$.

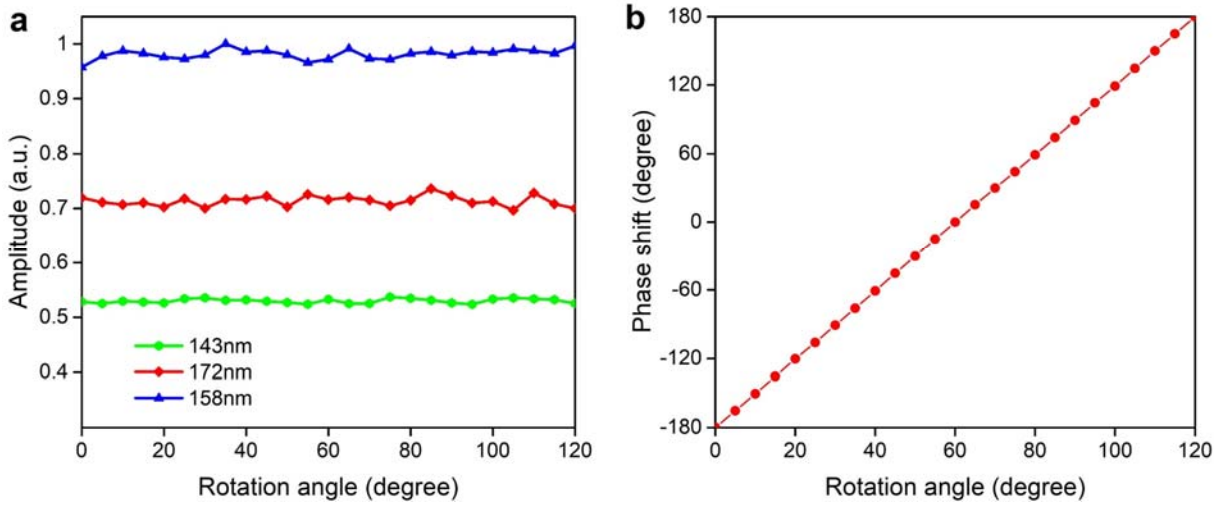

Figure S3. a) The variation of the amplitude of the generated SH waves with the changing of the rotation angle θ for the nanoparticles with arm lengths l = 143 nm, 172 nm and 158 nm respectively. b) The variation of the phase of the generated SH waves with the changing of the rotation angle θ for nanoparticle with arm lengths l = 158 nm.

Section 4. The calculated multichannel vortex beams generated by phase-only nonlinear metasurface

During the design of the phase-only metasurface, the phase of the metasurface can be expressed as $\phi = \arg(\sum_{k=1}^{n} a_k \exp(i\Phi_k))$. For geometric phase-only metasurfaces, their optical functionalities are conjugate for RCP and LCP illuminations since the geometric phase for RCP and LCP illuminations are opposite. Thus, if the optical functionality of the first sample (shown in Figure 3) is realized by geometric phase-only metasurfaces, the multichannel vortex beams can be generated at the real focal plane under RCP illumination while the same multichannel vortex beams can be generated at the virtual focal plane under LCP illumination, as shown in Figure S4. The advantages of our work compared with geometric phase-only metasurfaces is that the optical functionalities of the designed nonlinear metasurfaces are not conjugate for RCP and LCP illuminations, which provide a powerful platform for the realization of the spin-controlled multifunctional nonlinear metasurfaces.

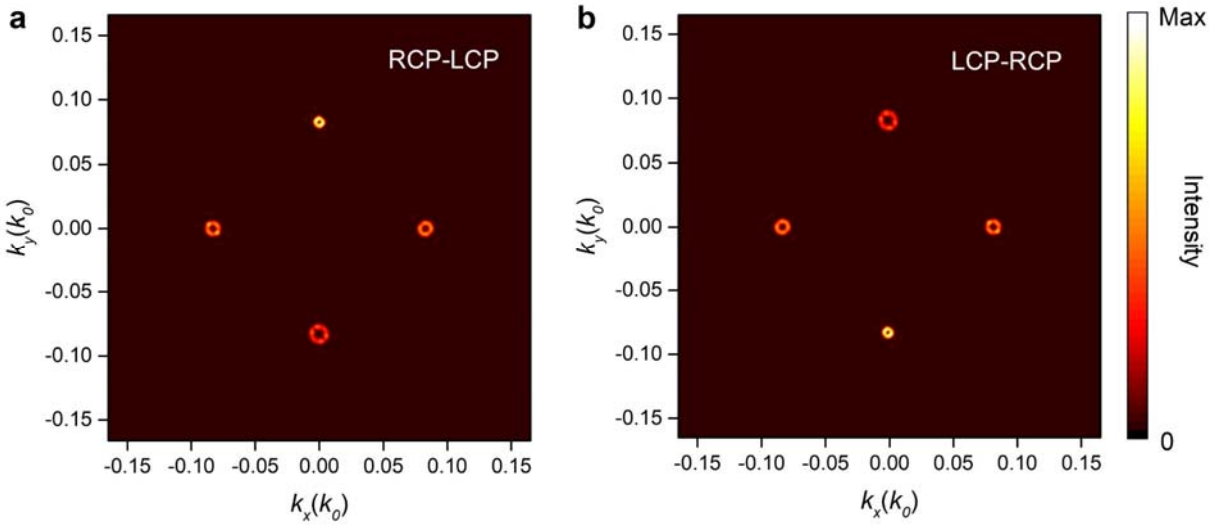

Figure S4. a) Calculated LCP light intensity distributions of SH waves in *k*-space at the real focal plane for RCP incidence. b) Calculated RCP light intensity distributions of SH waves in *k*-space at the virtual focal plane for LCP incidence.

Section 5. Spin-selective generation of four SH optical vortices with independent topological charges

We designed another sample with four channels for LCP illumination and set the focusing optical vortices F_1, F_2, F_3 and F_4 with topological charges $l_1 = +2$, $l_2 = -2$, $l_3 = +3$, and $l_4 = -1$, respectively. The corresponding numerical and experimental results are shown in Figure S5.

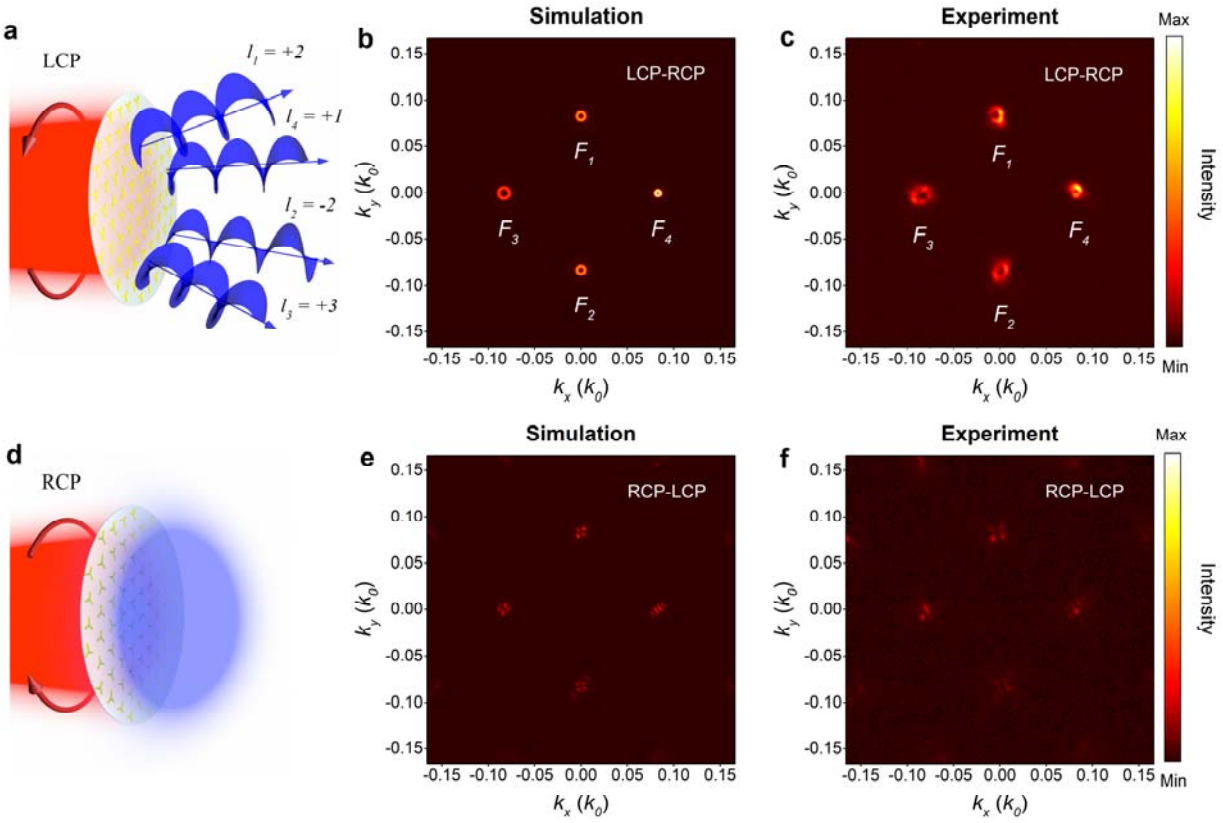

Figure S5. a) Schematic of the multichannel vortex beams with designed metasurface for LCP incidence. b) Calculated RCP light intensity distributions of SH waves in *k*-space at the real focal plane for LCP incidence. The four SH optical vortices channels, F_1, F_2, F_3 and F_4 were located at (0, $0.083k_0$), (0, $-0.083k_0$), ($-0.083k_0$, 0) and ($0.083k_0$, 0), respectively. c) Measured RCP light intensity distributions of SH waves in *k*-space at the real focal plane for LCP incidence. d) Schematic of the block channels for RCP incidence. Calculated (e) and measured (f) LCP intensity distribution at the virtual focal plane for RCP incidence.

Section 6. The design of the spin-controlled multifunctional nonlinear metasurface

The multifunctional metasurface consists of unit cells with different structural parameters that can realize the complex-amplitude modulation of SHG. The complex-amplitude profiles of the SH waves for the designed metasurface under LCP and RCP illuminations are shown in Figure S6. For RCP incidence, the metasurface can generate focusing optical vortices channels F_1 and F_2 with topological charges $l_1 = +1$ and $l_2 = +3$, while the multifunctional metasurface is designed to generate channels F_3 and F_4 with topological charges $l_3 = +2$ and $l_4 = -2$ under LCP illumination.

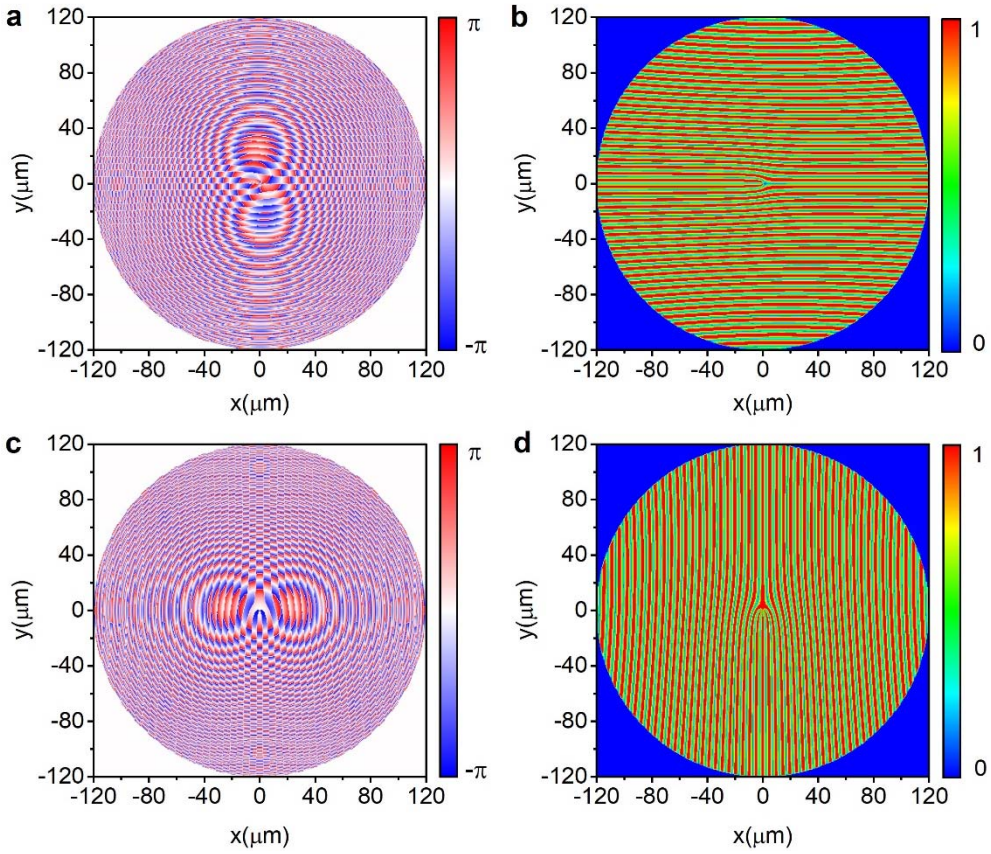

Figure S6. Calculated (a) phase profile and (b) five-level amplitude profile of RCP SH waves for the designed multifunctional metasurface under LCP illumination. Calculated (c) phase profile and (d) five-level amplitude profile of LCP SH waves for the designed multifunctional metasurface under RCP illumination.